Revealing thermally driven distortion of magnon dispersion by spin Seebeck effect in $Gd_3Fe_5O_{12}$

B. Yang,[1] S. Y. Xia,[1] H. Zhao,[1] G. Liu,[1] J. Du,[1] Ka Shen,[2,*] Zhiyong Qiu,[3,†] and D. Wu[1,‡]

[1]*National Laboratory of Solid State Microstructures, Jiangsu Provincial Key Laboratory for Nanotechnology, Collaborative Innovation Center of Advanced Microstructures and Department of Physics, Nanjing University, Nanjing 210093, China*

[2]*Center for Advanced Quantum Studies and Department of Physics, Beijing Normal University, Beijing 100875, China*

[3]*School of Materials Science and Engineering, Dalian University of Technology, Dalian 116024, China*

(Received 23 December 2020; revised 23 January 2021; accepted 25 January 2021; published 4 February 2021)

We report a systematic study of the temperature and field dependences of the spin Seebeck effect (SSE) in a bilayer of $Pt/Gd_3Fe_5O_{12}$. An anomalous structure is observed in the magnetic field dependent measurements at temperatures between ∼60 and ∼210 K. Unlike the ordinary SSE signal originating from the bare magnons, which changes sign at ∼95 and ∼266 K, the sign of the anomalies remains unchanged with increasing temperature. Moreover, the anomalies are found to show a temperature-sensitive double-peak structure between ∼116 and ∼143 K. We attribute these anomalies to the contribution from the quasiparticles hybridized between the Gd moment dominated spin wave (α mode) and the transversal acoustic phonon, known as the magnon polarons. Given that the magnon polaron induced anomalies occur at the field where the linear phonon dispersion is tangential to the magnon dispersion curve, we explain these rich phenomena by an increase of the group velocity of the α-mode magnon with increasing temperature and the nonparabolic magnon dispersion of $Gd_3Fe_5O_{12}$. Our results demonstrate that the magnon polaron induced SSE is helpful for the investigation of the magnon dispersion evolution with a simple transport approach.

DOI: 10.1103/PhysRevB.103.054411

I. INTRODUCTION

Magnon polarons are the quasiparticles of the hybridized magnon and phonon modes through magnetoelastic coupling [1,2]. The coupling strength reaches the maximum value at the intersections of the uncoupled magnon and phonon dispersion curves and rapidly decays away from the intersections. The magnon polarons have the mixed characteristics of the magnetic and lattice dynamics in the proximity of the intersection region. Recent investigations have demonstrated that the magnon polarons can play important roles in several magnon transport related phenomena such as the spin Seebeck effect (SSE) [3–11] and its reciprocal effect, the spin Peltier effect [12]; nonlocal measurements [13–15]; and spin pumping [16]. In addition to these studies, the magnon polarons provide an avenue to interconvert the angular momentum between the spin wave and the elastic wave [17].

The initial report of the magnon polaron enhanced SSE, which relies on the magnon transport upon the application of a temperature gradient, was discovered in the magnetic field dependent measurements in the bilayer of $Pt/Y_3Fe_5O_{12}$ (YIG) [3]. The enhancements occur at certain magnetic fields, where the transverse acoustic (TA) or longitudinal acoustic (LA) dispersion curves tangentially touch the magnon dispersion curve. At the "touching" fields, the magnon and phonon modes are coupled over the largest volume in the frequency space, leading to the strongest magnon-phonon coupling. Owing to the ratio of the magnon and phonon scattering potentials (η) being much larger than 1 for the high quality single-crystalline YIG, the lifetime of the magnon and the corresponding SSE are enhanced [9]. Given that η is independent of temperature, the contribution of the magnon polarons to the SSE, enhancement or reduction, would not change with temperature. Although YIG is a typical ferrimagnetic material [18,19], its magnon dispersion is generally considered to be parabolic with a single band in most experiments, particularly at low temperature [5,20–22], owing to the strong antiferromagnetic exchange interaction (∼3 eV) between the Fe atoms occupied at tetrahedral (d) and octahedral (a) sites and the large gap of ∼8 THz between magnon acoustic and optical modes below 100 K [23–25]. Similar magnon polaron induced anomalies were later observed in other magnetic insulators [4–7], including a very recent report in uniaxial antiferromagnetic insulator Cr_2O_3. Among these works, Ramos *et al.* [4] demonstrated the tunability of the magnon polaron induced anomaly by engineering the magnon dispersion via doping YIG. Very interestingly, a recent model calculation predicted that the anomaly of SSE in a special ferrimagnetic insulator $Gd_3Fe_5O_{12}$ (GdIG) can be efficiently manipulated solely by tuning the temperature and can exhibit rich features in sharp contrast with that observed in YIG and all other materials [8]. However, to date, corresponding experimental studies in GdIG are rare, which motivates the present work.

Therefore, we perform systematic measurements of the SSE in a bilayer consisting of a GdIG and a heavy metal Pt. It is well known that the behavior of the SSE in Pt/GdIG is completely different from that in Pt/YIG [26]. Due to the negligible exchange interaction between Gd atoms and weak antiferromagnetic exchange interaction between Gd and Fe

*kashen@bnu.edu.cn
†qiuzy@dlut.edu.cn
‡dwu@nju.edu.cn

atoms, the magnetization of the Gd sublattice is much more sensitive to temperature than that of the Fe sublattices [27,28]. As a result, the total magnetic moment vanishes at the compensation temperature (T_{comp}), at which the sign of the SSE signal changes [26,29]. Another SSE sign change is observed below T_{comp}. It is interpreted by the increase of spin injection efficiency of the Fe moment dominated spin wave modes (β mode) at high temperature, which generate the opposite spin current to compensate that from the Gd moment dominated spin wave modes (α mode) dominated at low temperature [26]. These distinctive behaviors of the SSE in GdIG, the magnon polarons in GdIG, might reveal more physics of the coupling between magnon and phonon than other materials.

In this work, we report our direct observation of the anomalous structures in the longitudinal SSE measurements induced by magnon polarons in Pt/GdIG. Unlike the reported anomalies in Pt/YIG and other systems, the positions and line shapes of the anomalies strongly depend on temperature and field. Furthermore, the sign of the anomalies remains unchanged with increasing temperature in comparison with two sign changes of the ordinary SSE at ~95 and ~266 K. Since the ordinary SSE is mainly contributed by the α mode at low temperature and the sign change of the ordinary SSE is caused by the predominant contribution of the β mode above ~95 K [26], we infer that the α mode participates in the formation of the magnon polaron. Our observations are consistent with a qualitative analysis based on the previously reported finite-temperature calculation of the α mode in GdIG, and thus provide transport evidence of the thermally driven distortion of its dispersion.

II. EXPERIMENT

The single-crystalline GdIG films with a thickness of about 3 μm were grown on $Gd_3Ga_5O_{12}$ (GGG) (111) substrates by liquid phase epitaxy. The magnetic properties were measured by a superconducting quantum interference device vibrating sample magnetometer (SQUID-VSM, Quantum Design). The 5 nm thick Pt films, patterned into a 0.3 mm wide and 2.6 mm long Hall bar by a metallic mask, were deposited on GdIG film by a dc sputtering system at room temperature. The base pressure was 2.6×10^{-5} Pa and Ar pressure was about 0.1 Pa during the deposition. The longitudinal SSE voltage [30–42] in the Pt/GdIG bilayer was measured by a nanovoltmeter (2182A, Keithley) in a physical properties measurement system (PPMS, Quantum Design). The resistances of the Pt film and the resistor close to the sample were measured simultaneously using the four-probe method.

The crystal quality of the samples was examined by x-ray diffraction (XRD). The XRD $\omega - 2\theta$ scan of the GdIG/GGG (111) sample is shown in Fig. 1(a). The out of plane lattice constant of the GdIG film is determined to be 12.47 Å, consistent with the bulk value for the very thick film [43,44]. This, together with the very strong (444) reflection peak from the GdIG film, indicates the good quality of the GdIG film.

III. RESULTS AND DISCUSSION

The typical hysteresis loops measured on our GdIG film at various temperatures with scanning an in-plane magnetic field are shown in Fig. 1(b). Obviously, the saturation magnetization (M_S) changes nonmonotonically with increasing temperature. To obtain T_{comp}, the magnetization as a function of temperature recorded at a magnetic field of 0.05 T measured by SQUID is plotted in Fig. 1(c). $T_{comp} = \sim 272$ K, lower than T_{comp} of bulk GdIG (~288 K), is estimated from the temperature at which the magnetization exhibits a minimum value. A similar T_{comp} decrease of the GdIG film has been reported and attributed to strain effects and slightly off stoichiometry [26,45].

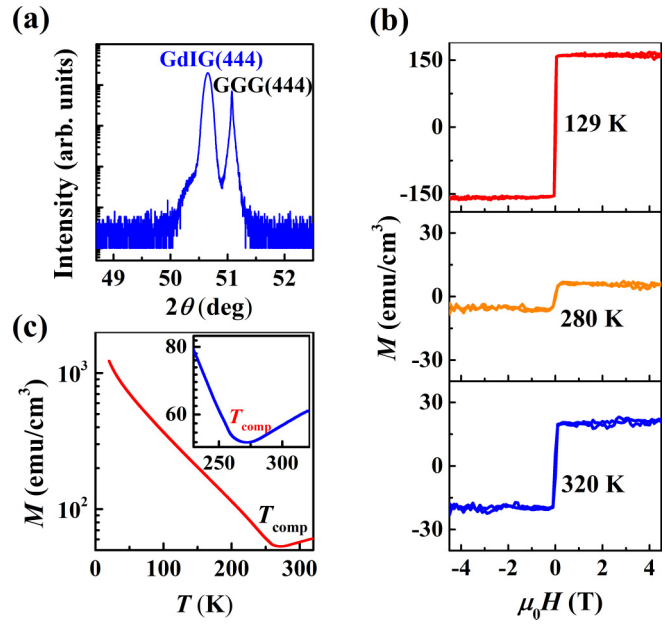

FIG. 1. (a) The XRD $\omega - 2\theta$ scan of the GdIG/GGG (111) film. (b) The typical hysteresis loops measured on the GdIG film at three typical temperatures. (c) The magnetization as a function of temperature measured at a magnetic field of 0.05 T. The inset is the blowup around T_{comp}.

We adopted the longitudinal SSE measurement geometry. The experimental geometry is shown in Fig. 2(a). The sample with a resistive heater on the top of the sample surface is mounted on a copper holder as a heat sink, where there is a layer of thermally conductive adhesive between the sample and the heater to enhance the heat transfer efficiency. A resistor was attached near the sample to measure the heater sink temperature (T_L) via its temperature-dependent electrical resistance. The temperature of the GdIG surface (T_H) was accurately measured via the temperature-dependent electrical resistance of the Hall bar of the Pt film, which also serves as the spin current detector. The generated temperature difference (ΔT) perpendicular to the sample plane is obtained as $\Delta T = T_H - T_L$. Because the thickness of the Pt/GdIG bilayer is two orders of magnitude smaller than that of the GGG substrate, T_H is very close to the average temperature of the Pt/GdIG bilayer and hence we consider the sample temperature T to be equal to T_H. The directions of ΔT (z direction), the applied in-plane magnetic field (H) (x direction), and the detection of the SSE voltage (V) (y direction) are always perpendicular to each other to obtain the maximum SSE signal in all measurements. As shown in Fig. 2(b), V is recorded

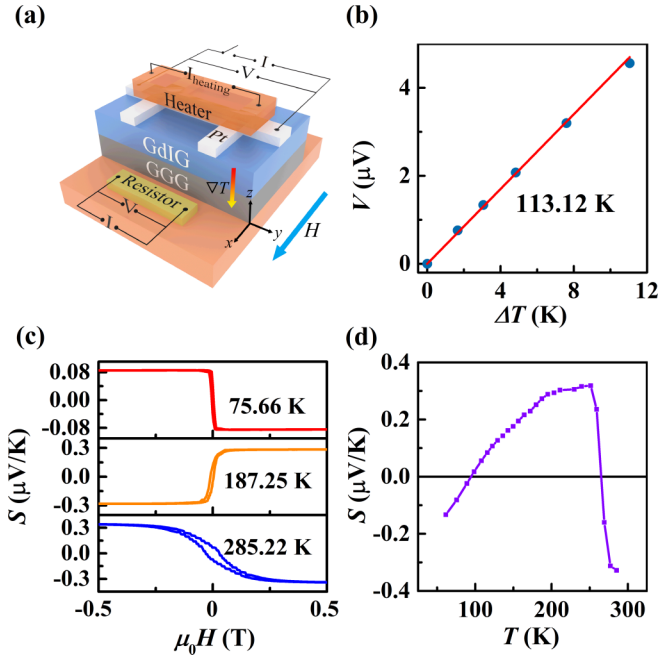

FIG. 2. (a) Measurement geometry of the SSE in Pt/GdIG/GGG sample. (b) V as a function of ΔT for the Pt/GdIG/GGG sample at $\mu_0 H = 0.2$ T. (c) S as a function of magnetic field for Pt/GdIG/GGG sample at 75.66, 187.25, and 285.22 K, respectively. (d) Temperature dependence of S for Pt/GdIG/GGG sample.

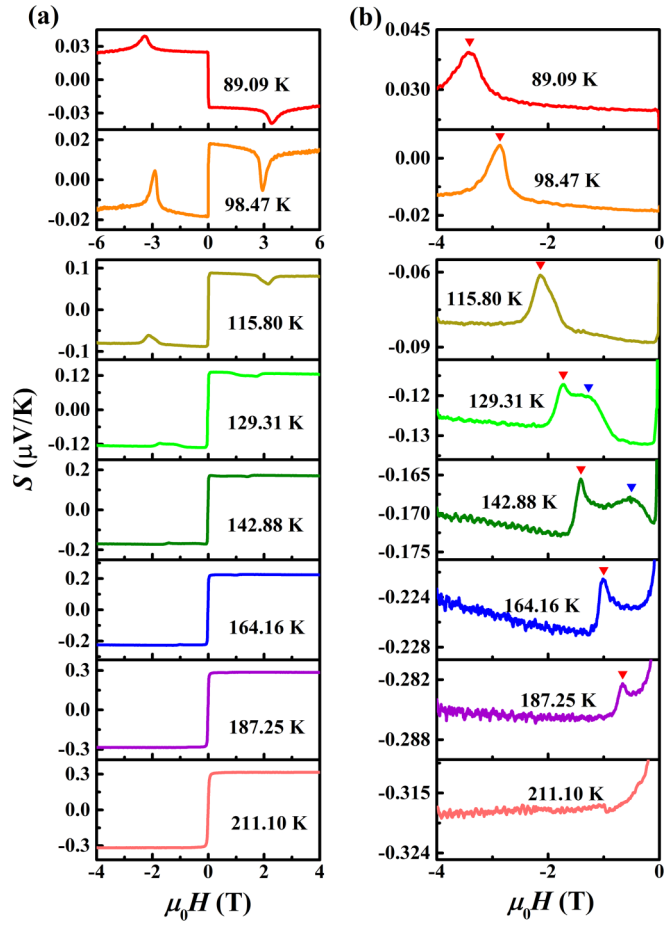

FIG. 3. (a) S of the Pt/GdIG/GGG sample measured at different temperatures. (b) The corresponding blowups of S at different temperatures.

as a function of ΔT at $\mu_0 H = 0.2$ T and $T = 113.12$ K which is controlled by both the cryostat and the heater to remain unchanged. It exhibits a linear dependence passing through the origin, suggesting that V originates from the SSE. This allows us to calculate the normalized SSE voltage $S = (V/\Delta T)/(L_y/L_z)$, where $L_z = 0.5$ mm is the thickness of the GdIG/GGG film and $L_y = 2.6$ mm is the length of the Pt film to detect the SSE voltage. The temperature gradient is not a constant value across the whole sample because of the different thermal conductivities of GGG and GdIG, meaning that $\Delta T/L_z$ and S do not represent the actual temperature gradient in the GdIG film and magnitude of the SSE coefficient, respectively. Even so, S still qualitatively describes the behavior of the SSE well.

Figure 2(c) shows S as a function of magnetic field measured at three typical temperatures with $\mu_0 H \leqslant 0.5$ T. The hysteretic S clearly exhibits sign change twice with increasing temperature, in sharp contrast from that of the Pt/YIG system. To evaluate the variation of S as a function of temperature, we extract S at $\mu_0 H = 0.3$ T, larger than the saturation field, in all field-dependent measurement data and plot them in Fig. 2(d). S shows very strong temperature dependence in magnitude and sign. The sign of S is negative at low temperature and changes to positive around $T_1 = 95$ K, then the magnitude of S increases with gradual increase of temperature. At around $T_2 \approx T_{\text{comp}}$, S exhibits an abrupt sign change from positive to negative without changing its magnitude too much. These results are consistent with previous reports [26].

In order to explore the role of magnon polarons, we carried out the field-dependent SSE measurements at various temperatures. The results are shown in Fig. 3(a), where the contributions from the ordinary magneto-Seebeck effect have been removed (see Supplemental Material [46]). We observe anomalous peak structures on top of the ordinary SSE signal in the data measured between 61.44 and 211.10 K. To clearly see the line shape of the structures, the corresponding enlarged plots around the structures are shown in Fig. 3(b). At first glance, the anomalous peaks look quite similar to those previously observed in Pt/YIG [3], Pt/Fe_3O_4 [6], and $Pt/Ni_{0.65}Zn_{0.35}Al_{0.8}Fe_{1.2}O_4$ [5] and are attributed to the magnon polarons, suggesting the same magnon-polaron origin of our present anomalous feature. On the other hand, the unique magnetic properties in GdIG lead to distinctive behaviors.

For $T < T_1$, the anomalies have the same sign with the ordinary SSE, meaning that the SSE signal is enhanced by the magnon polarons, similar to the Pt/YIG system. In this temperature range, the contribution of the α mode to the SSE predominates over that of the β mode. Therefore, we infer that the observed anomalies stem from the hybridization of the α mode with the phonon. Meanwhile, considering that the magnon hybridizes with the TA phonon at a smaller wave vector than the LA phonon because of the slower sound velocity of the TA phonon, the sole anomalous peak in our experimental field range can be attributed to the hybridization

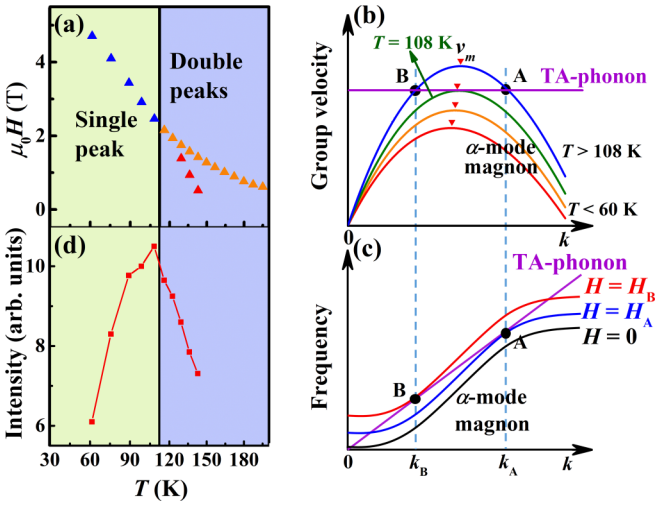

FIG. 4. (a) The positions of the anomalous peaks as a function of temperature for Pt/GdIG/GGG sample. For $T \leqslant \sim 108$ K, only one peak appears. For ~ 108 K $< T < \sim 129$ K, the anomalies display a double-peak shape. However, only one peak position can be determined. For ~ 129 K $\leqslant T \leqslant \sim 143$ K, the positions of both peaks can be resolved. For $T > \sim 143$ K, only one peak is observed and the other peak is not observable due to the rapid change of the background signal around the coercivity field. (b) The schematic diagram of the group velocities of the α-mode magnon and TA phonon as a function of wave vector at different temperatures of GdIG film. (c) The schematic diagram of dispersion relations of the α-mode magnon and TA phonon for $T > \sim 108$ K. The black, blue, and red solid curves represent the dispersion curves of the α-mode magnon when the applied field is 0, H_A, and H_B, respectively. (d) Temperature dependence of the intensity of the anomalous structures.

of the α-mode magnon with the TA phonon rather than the LA phonon. However, for $T_1 < T < \sim 210$ K, the anomalies that originated from the magnon polarons do not change sign with the ordinary SSE signal which comes from the bare magnons, resulting in the reduction of the SSE signal. The shapes, amplitudes, and positions of the anomalies do not have abrupt change across T_1, suggesting that the anomalies in this temperature range have the same origin as the anomalies appearing at low temperature. That is to say, the α mode still produces the negative SSE signal and the positive SSE signal comes from another magnon mode. This result further validates the explanation of the SSE sign change at T_1, which is that the β mode dominates the SSE above T_1. For $T > \sim 210$ K, the anomalies appear at the field close to the coercivity field and become unrecognizable due to the rapid change of the background signal with field.

Figure 4(a) shows the positions of the anomalous peaks as a function of temperature. Comparing with the Pt/YIG system reported in Ref. [3], there are two distinct differences. First, the position of the anomalous peak rapidly shifts to the lower fields with increasing temperature [Fig. 3(b)], whereas the shift of the position of the anomalous peak in Pt/YIG is very small. The anomalies emerge at the fields where the phonon dispersion is tangential to the magnon dispersion to maximize the phase space of the magnon-polaron coupling. Since the phonon dispersion is almost independent of temperature, this observation reflects that the magnon dispersion varies with temperature significantly due to the very weak exchange interaction between Gd and Fe ($\sim$0.16 meV) [27,47]. Second, the anomalies display a double-peak shape from ~ 116 K and the double peaks are clearly separated with an increasing spacing from ~ 129 K [Fig. 3(b)]. The strong temperature sensitivity of the peak splitting reveals that the double peaks in our Pt/GdIG have a different origin from that in Pt/YIG, where the double peaks correspond to the tangential intersections of the magnon dispersion with the TA- and LA-phonon dispersions, respectively. Similar double-peak structures were observed in $Pt/Ni_{0.65}Zn_{0.35}Al_{0.8}Fe_{1.2}O_4$ (NZA ferrite) and attributed to the intersection of the quantized magnon and phonon dispersions. According to this mechanism, two peaks should have similar line shapes and the relative positions of the two peaks should remain unchanged with increasing temperature. Our sample, however, does not show these characteristics, meaning that these mechanisms should be irrelevant to our present observations in Pt/GdIG.

Our findings can be qualitatively explained by the distortion of the magnon dispersion driven by the thermal excitation [8]. Both first-principle calculations and model calculations show that the dispersion of the α mode in GdIG is parabolic only around the Γ point and becomes very weak around the Brillouin zone boundary [8,27]. As a result, the group velocity, the derivative of the dispersion curve, of the α mode is nearly zero at both the Γ point and the Brillouin zone boundary, and arrives at a maximum value (v_m) at a certain intermediate wave vector, as schematically shown in Fig. 4(b). Below $\sim$60 K, v_m is much smaller than the TA-phonon sound velocity (v_{TA}), meaning that the tangential intersection cannot take place at any magnetic field and hence the anomaly is absent. v_m increases with increasing temperature according to the calculations [8]. Therefore, when the temperature increases to $\sim$60 K, v_m is close to v_{TA}. By applying a magnetic field, the magnon dispersion rigidly shifts to a high frequency such that the TA phonon could become nearly tangential to the magnon dispersion at a certain field, leading to the weakly coupled magnon-phonon. As a result, the single-peak anomaly appears. With increasing temperature further, the coupling strength gets stronger by approaching the tangential situation, leading to the increase of the intensity of the anomaly, as shown in Fig. 4(d), where the intensity is the absolute value of the integration of the anomalous structure after subtracting the background (see Supplemental Material [46]). The strongest coupling strength or intensity of the single-peak anomaly indicates the achievement of the tangential situation, $v_m = v_{TA}$, which occurs at $T \approx 108$ K.

For $T > \sim 108$ K, the group velocities of the magnon and TA phonon have two crossing points (A and B) at k_A and k_B, as shown in Fig. 4(c), which means the slopes of the magnon and phonon dispersions are equal at k_A and k_B. As increasing the field, the magnon dispersion curve shifts upward and must become tangential to the phonon dispersion at k_A at a certain field H_A, leading to an appearance of the first peak. With further increasing the field, the magnon dispersion curve would tangentially intersect with the phonon dispersion curve at k_B at a certain field H_B and hence the second peak emerges. The peak to peak spacing gets larger with increasing temperature because of the upward shift of the magnon group velocity curve. Since the coupling strength relies on the overlapped

volume of the magnon and phonon modes in the momentum-frequency space, we can estimate the coupling strength by the difference between the first derivative of the magnon and phonon group velocities. Given that the first derivative of the phonon group velocity is zero, the increase of the first derivative of the magnon group velocity with increasing temperature [Fig. 4(b)] leads to the reduction of the coupling strength. Therefore, the intensity of the double-peak anomaly decreases with increasing temperature. As a consequence, the total intensity of the peaks arrives at a maximum at the critical temperature where the double-peak anomalous structure emerges, as shown in Fig. 4(d). Above ∼150 K, we do not analyze the intensity further because the strong background signal does not allow us to accurately calculate the intensity of the anomalous structure.

IV. CONCLUSIONS

In summary, we observe anomalous structures in the field-dependent SSE measurements from 61.44 to 211.10 K in Pt/GdIG. The anomalies are attributed to the magnon polaron mode which is the hybridization of the Gd moment dominated spin wave and the TA phonon. The position, intensity, and shape of the anomalies strongly depend on temperature, very different from the typical magnetic insulator YIG and other magnetic insulators. A phenomenal model of the increase of the magnon group velocity with increasing temperature can qualitatively explain our observation. Our results show that the magnon polaron SSE promises to provide the information of the magnon dispersion, which is crucial for the magnonic applications.

ACKNOWLEDGMENTS

This work was financially supported by National Natural Science Foundation of China (Grants No. 52025012, No. 11974047, No. 11727808, and No. 51971109), National Key R&D Program of China (2017YFA0303202), and the Fundamental Research Funds for the Central Universities (2018EYT02).

[1] A. Kamra, H. Keshtgar, P. Yan, and G. E. W. Bauer, Coherent elastic excitation of spin waves, Phys. Rev. B **91**, 104409 (2015).

[2] K. Shen and G. E. W. Bauer, Laser-Induced Spatiotemporal Dynamics of Magnetic Films, Phys. Rev. Lett. **115**, 197201 (2015).

[3] T. Kikkawa, K. Shen, B. Flebus, R. A. Duine, K. I. Uchida, Z. Qiu, G. E. W. Bauer, and E. Saitoh, Magnon Polarons in the Spin Seebeck Effect, Phys. Rev. Lett. **117**, 207203 (2016).

[4] R. Ramos, T. Hioki, Y. Hashimoto, T. Kikkawa, P. Frey, A. J. E. Kreil, V. I. Vasyuchka, A. A. Serga, B. Hillebrands, and E. Saitoh, Room temperature and low-field resonant enhancement of spin Seebeck effect in partially compensated magnets, Nat. Commun. **10**, 5162 (2019).

[5] H. Wang, D. Hou, T. Kikkawa, R. Ramos, K. Shen, Z. Qiu, Y. Chen, M. Umeda, Y. Shiomi, X. Jin, and E. Saitoh, The bimodal distribution spin Seebeck effect enhancement in epitaxial $Ni_{0.65}Zn_{0.35}Al_{0.8}Fe_{1.2}O_4$ thin film, Appl. Phys. Lett. **112**, 142406 (2018).

[6] W. Xing, Y. Ma, Y. Yao, R. Cai, Y. Ji, R. Xiong, K. Shen, and W. Han, Facet-dependent magnon-polarons in epitaxial ferrimagnetic Fe_3O_4 thin films, Phys. Rev. B **102**, 184416 (2020).

[7] J. Li, H. T. Simensen, D. Reitz, Q. Sun, W. Yuan, C. Li, Y. Tserkovnyak, A. Brataas, and J. Shi, Observation of Magnon Polarons in a Uniaxial Antiferromagnetic Insulator, Phys. Rev. Lett. **125**, 217201 (2020).

[8] K. Shen, Temperature-switched anomaly in the spin Seebeck effect in $Gd_3Fe_5O_{12}$, Phys. Rev. B **99**, 024417 (2019).

[9] B. Flebus, K. Shen, T. Kikkawa, K.-I. Uchida, Z. Qiu, E. Saitoh, R. A. Duine, and G. E. W. Bauer, Magnon-polaron transport in magnetic insulators, Phys. Rev. B **95**, 144420 (2017).

[10] R. Schmidt, F. Wilken, T. S. Nunner, and P. W. Brouwer, Boltzmann approach to the longitudinal spin Seebeck effect, Phys. Rev. B **98**, 134421 (2018).

[11] W. Han, S. Maekawa, and X.-C. Xie, Spin current as a probe of quantum materials, Nat. Mater. **19**, 139 (2020).

[12] R. Yahiro, T. Kikkawa, R. Ramos, K. Oyanagi, T. Hioki, S. Daimon, and E. Saitoh, Magnon polarons in the spin Peltier effect, Phys. Rev. B **101**, 024407 (2020).

[13] J. Shan, A. V. Singh, L. Liang, L. J. Cornelissen, Z. Galazka, A. Gupta, B. J. van Wees, and T. Kuschel, Enhanced magnon spin transport in $NiFe_2O_4$ thin films on a lattice-matched substrate, Appl. Phys. Lett. **113**, 162403 (2018).

[14] L. J. Cornelissen, K. Oyanagi, T. Kikkawa, Z. Qiu, T. Kuschel, G. E. W. Bauer, B. J. van Wees, and E. Saitoh, Nonlocal magnon-polaron transport in yttrium iron garnet, Phys. Rev. B **96**, 104441 (2017).

[15] B. Z. Rameshti and R. A. Duine, Length scale for magnon-polaron formation from nonlocal spin transport, Phys. Rev. B **99**, 060402(R) (2019).

[16] H. Hayashi and K. Ando, Spin Pumping Driven by Magnon Polarons, Phys. Rev. Lett. **121**, 237202 (2018).

[17] J. Holanda, D. Maior, A. Azevedo, and S. Rezende, Detecting the phonon spin in magnon–phonon conversion experiments, Nat. Phys. **14**, 500 (2018).

[18] S. Geprägs, S. Meyer, S. Altmannshofer, M. Opel, F. Wilhelm, A. Rogalev, R. Gross, and S. T. B. Goennenwein, Investigation of induced Pt magnetic polarization in $Pt/Y_3Fe_5O_{12}$ bilayers, Appl. Phys. Lett. **101**, 262407 (2012).

[19] D. Rodic, M. Mitric, R. Tellgren, H. Rundlof, and A. Kremenovic, True magnetic structure of the ferrimagnetic garnet $Y_3Fe_5O_{12}$ and magnetic moments of iron ions, J. Magn. Magn. Mater. **191**, 137 (1999).

[20] K. Shen, Finite temperature magnon spectra in yttrium iron garnet from a mean field approach in a tight-binding model, New J. Phys. **20**, 043025 (2018).

[21] H. Jin, S. R. Boona, Z. Yang, R. C. Myers, and J. P. Heremans, Effect of the magnon dispersion on the longitudinal spin Seebeck effect in yttrium iron garnets, Phys. Rev. B **92**, 054436 (2015).

[22] S. R. Boona and J. P. Heremans, Magnon thermal mean free path in yttrium iron garnet, Phys. Rev. B **90**, 064421 (2014).

[23] L. S. Xie, G. X. Jin, L. X. He, G. E. W. Bauer, J. Barker, and K. Xia, First-principles study of exchange interactions of yttrium iron garnet, Phys. Rev. B **95**, 014423 (2017).

[24] Y. Nambu, J. Barker, Y. Okino, T. Kikkawa, Y. Shiomi, M. Enderle, T. Weber, B. Winn, M. Graves-Brook, J. M. Tranquada, T. Ziman, M. Fujita, G. E. W. Bauer, E. Saitoh, and K. Kakurai, Observation of Magnon Polarization, Phys. Rev. Lett. **125**, 027201 (2020).

[25] J. S. Plant, Spinwave dispersion curves for yttrium iron garnet, J. Phys. C: Solid State Phys. **10**, 4805 (1977).

[26] S. Geprgäs *et al.*, Origin of the spin Seebeck effect in compensated ferrimagnets, Nat. Commun. **7**, 10452 (2016) .

[27] L.-W. Wang, L.-S. Xie, P.-X. Xu, and K. Xia, First-principles study of magnon-phonon interactions in gadolinium iron garnet, Phys. Rev. B **101**, 165137 (2020).

[28] F. Söderlind, L. Selegård, P. Nordblad, K. Uvdal, and P.-O. Käll, Sol–gel synthesis and characterization of polycrystalline $GdFeO_3$ and $Gd_3Fe_5O_{12}$ thin films, J. Sol-Gel Sci. Technol. **49**, 253 (2009).

[29] J. Cramer, E.-J. Guo, S. Geprägs, A. Kehlberger, Y. P. Ivanov, K. Ganzhorn, F. Della Coletta, M. Althammer, H. Huebl, R. Gross, J. Kosel, M. Kläui, and S. T. B. Goennenwein, Magnon mode selective spin transport in compensated ferrimagnets, Nano Lett. **17**, 3334 (2017).

[30] T. Kikkawa, K. Uchida, S. Daimon, Z. Qiu, Y. Shiomi, and E. Saitoh, Critical suppression of spin Seebeck effect by magnetic fields, Phys. Rev. B **92**, 064413 (2015).

[31] K. Uchida, T. Nonaka, T. Ota, and E. Saitoh, Longitudinal spin-Seebeck effect in sintered polycrystalline $(Mn,Zn)Fe_2O_4$, Appl. Phys. Lett. **97**, 262504 (2010).

[32] G. Siegel, M. C. Prestgard, S. Teng, and A. Tiwari, Robust longitudinal spin-Seebeck effect in Bi-YIG thin films, Sci. Rep. **4**, 4429 (2014).

[33] H. Kannan, X. Fan, H. Celik, X. Han, and J. Q. Xiao, Thickness dependence of anomalous Nernst coefficient and longitudinal spin Seebeck effect in ferromagnetic Ni_xFe_{100-x} films, Sci. Rep. **7**, 6175 (2017).

[34] K. Uchida, M. Ishida, T. Kikkawa, A. Kirihara, T. Murakami, and E. Saitoh, Longitudinal spin Seebeck effect: from fundamentals to applications, J. Phys.: Condens. Matter **26**, 343202 (2014).

[35] K. Uchida, T. Kikkawa, A. Miura, J. Shiomi, and E. Saitoh, Quantitative Temperature Dependence of Longitudinal Spin Seebeck Effect at High Temperatures, Phys. Rev. X **4**, 041023 (2014).

[36] K. Uchida, T. Nonaka, T. Kikkawa, Y. Kajiwara, and E. Saitoh, Longitudinal spin Seebeck effect in various garnet ferrites, Phys. Rev. B **87**, 104412 (2013).

[37] R. Iguchi, K. I. Uchida, S. Daimon, and E. Saitoh, Concomitant enhancement of the longitudinal spin Seebeck effect and the thermal conductivity in a Pt/YIG/Pt system at low temperatures, Phys. Rev. B **95**, 174401 (2017).

[38] U. Ritzmann, D. Hinzke, A. Kehlberger, E.-J. Guo, M. Kläui, and U. Nowak, Magnetic field control of the spin Seebeck effect, Phys. Rev. B **92**, 174411 (2015).

[39] A. Sola, M. Kuepferling, V. Basso, M. Pasquale, T. Kikkawa, K. Uchida, and E. Saitoh, Evaluation of thermal gradients in longitudinal spin Seebeck effect measurements, J. Appl. Phys. **117**, 17C510 (2015).

[40] M. Agrawal, V. I. Vasyuchka, A. A. Serga, A. Kirihara, P. Pirro, T. Langner, M. B. Jungfleisch, A. V. Chumak, E. Th. Papaioannou, and B. Hillebrands, Role of bulk-magnon transport in the temporal evolution of the longitudinal spin-Seebeck effect, Phys. Rev. B **89**, 224414 (2014).

[41] K. Uchida, H. Adachi, T. Ota, H. Nakayama, S. Maekawa, and E. Saitoh, Observation of longitudinal spin-Seebeck effect in magnetic insulators, Appl. Phys. Lett. **97**, 172505 (2010).

[42] J. Li, Z. Shi, V. H. Ortiz, M. Aldosary, C. Chen, V. Aji, P. Wei, and J. Shi, Spin Seebeck Effect from Antiferromagnetic Magnons and Critical Spin Fluctuations in Epitaxial FeF_2 Films, Phys. Rev. Lett. **122**, 217204 (2019).

[43] G. P. Espinosa, Crystal chemical study of the rareearth iron garnets, J. Chem. Phys. **37**, 2344 (1962).

[44] P. R. Rovani, A. S. Ferreira, A. S. Pereira1, and J. C. de Lima, Effect of pressure on nanostructured $Gd_3Fe_5O_{12}$, J. Appl. Phys. **122**, 035904 (2017).

[45] B. W. Dong, J. Cramer, K. Ganzhorn, H. Y. Yuan, E. J. Guo, S. T. B. Goennenwein, and M. Klaui, Spin Hall magnetoresistance in the non-collinear ferrimagnet GdIG close to the compensation temperature, J. Phys.: Condens. Matter **30**, 035802 (2018).

[46] See Supplemental Material at http://link.aps.org/supplemental/10.1103/PhysRevB.103.054411 for ordinary magneto-Seebeck contribution to SSE and estimation of the intensity of the anomalous structure.

[47] C. M. Srivastava, Exchange constants in ferrimagnetic garnets, J. Appl. Phys. **53**, 781 (1982).